Semi-analytical solution of the time-dependent heat equation for three-dimensional anisotropic multi-layered media

Dominik Reitzle[a,*], Simeon Geiger[a], Alwin Kienle[a]

[a] *Institut für Lasertechnologien in der Medizin und Meßtechnik an der Universität Ulm, Helmholtzstr. 12, D-89081, Ulm, Germany*

Abstract

In this paper, a semi-analytical solution of the time-dependent heat conduction equation is presented for laterally infinite, multi-layered media with anisotropic thermal conductivities, convective outer boundaries and perfect thermal contact between the layers. Space and time-dependent moving heat sources on the boundary as well as inside the medium are considered. In addition, the outer fluid temperature may also depend on space and time. The derived solutions are successfully compared to numerical solutions. A Python implementation of the solution is made freely available.

Keywords: Heat conduction; semi-analytical; layered media; transient; anisotropic; moving source

1. Introduction

Heat conduction in functionally graded or coated materials plays an important role in many fields of engineering and science [1–3]. Many novel coating materials also exhibit a strongly anisotropic thermal conductivity [4, 5]. For example, tool coatings could be designed with an anisotropic thermal conductivity to alleviate problems due to high temperature and thermal stress [6]. The ability to accurately predict the time-dependent heat distribution and flow inside three-dimensional multi-layered media with anisotropic

*Corresponding author.
E-mail address: dominik.reitzle@ilm-ulm.de

thermal conductivities is therefore essential. Analytically solving the time-dependent heat equation for such a system has however proven difficult. Existing analytical or semi-analytical solutions [7–11] are therefore limited to e.g. one or two dimensions, isotropic heat conductivity, or the steady-state case. Recently, Zhang *et al.* used explicit closed-form frequency response functions combined with the Fast Fourier Transform (FFT) as an efficient numerical inverse transform [11] to solve the heat equation. This led to a reasonably efficient 3D semi-analytical solution for N layers with an arbitrarily shaped moving source on the upper medium boundary, but is limited to the steady-state case, isotropic thermal conductivities and a semi-infinite geometry. Following the same basic approach, we propose a semi-analytical time-resolved solution for a multi-layered slab with anisotropic thermal conductivities. We also consider sources inside the medium and an outer fluid temperature that may change with time and position.
In Section 2, we present the mathematical formulation of the problem with the imposed boundary and initial conditions and its solution in transformed space. We then briefly describe the numerical transform methods in section 3. Finally, we present a few exemplary results in section 4, compare them to a purely numerical reference method and close with a short summary and a few remarks on the numerical performance of the proposed solution.

2. Analytic solution in Fourier-Laplace space

2.1. Frequency domain solution

Figure 1 illustrates the problem geometry. N laterally infinite slabs labeled by $n = 1, ..., N$ are stacked on top of each other. The origin of the common z-axis is located at the top surface with positive direction as indicated. Each layer has a certain thickness $L^{(n)}$ and a set of material parameters consisting of the density $\rho^{(n)}$, the heat capacity $c_p^{(n)}$ and the thermal conductivity tensor $\mathbf{K}^{(n)}$. The thermal conductivity tensors are assumed symmetric with the components

$$\mathbf{K}^{(n)} = \begin{bmatrix} k_x^{(n)} & k_{xy}^{(n)} & k_{xz}^{(n)} \\ k_{xy}^{(n)} & k_y^{(n)} & k_{yz}^{(n)} \\ k_{xz}^{(n)} & k_{yz}^{(n)} & k_z^{(n)} \end{bmatrix}. \tag{1}$$

We consider a source plane with a spatial strength profile $Q_s(x, y)$ at depth $z = z_0$ inside layer m that is switched on at time $t = 0$ and then varies with

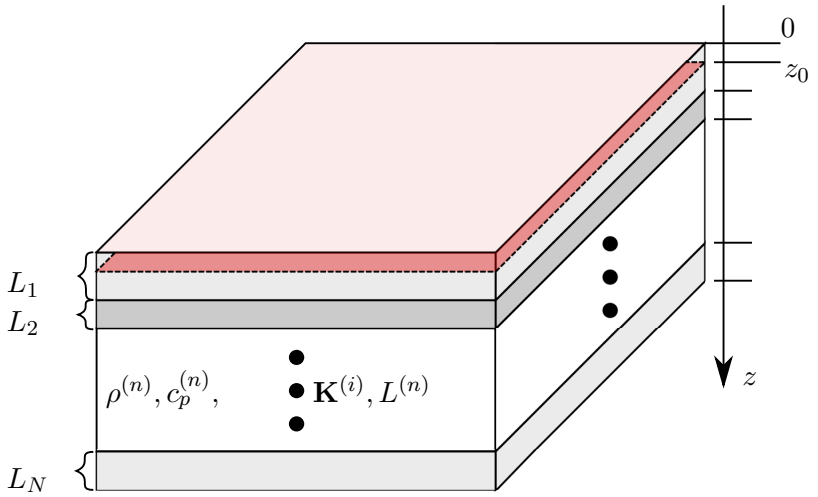

Figure 1: Schematic view of the considered geometry. The lateral dimension of the medium is infinite. The plane at $z = z_0$ contains the heat sources.

time according to $Q_t(t)$. If this source plane is placed exactly on the upper or lower medium boundary, this corresponds to a prescribed heat flux through the respective boundary. The heat transport inside each layer n can then be described by the differential equation

$$\rho^{(n)} c_p^{(n)} \frac{\partial T}{\partial t} - \nabla \cdot \left(\mathbf{K}^{(n)} \nabla T \right) = \delta_{nm} Q_s(x, y) \delta(z - z_0) Q_t(t) \Theta(t). \tag{2}$$

We use $T = 0$ everywhere as initial condition. Applying a 2D Fourier transform with respect to the spatial coordinates x and y and a Laplace transform with respect to time, we obtain (omitting the layer index n)

$$\frac{\partial^2}{\partial z^2} T + 2i\beta \frac{\partial}{\partial z} T - \alpha^2 T = -\delta_{nm} \frac{1}{k_z} \tilde{Q}_s(q_x, q_y) \tilde{Q}_t(s) \delta(z - z_0), \tag{3}$$

with the transformed spatial coordinates q_x and q_y and the Laplace variable s, where we introduced the variables α and β as

$$\alpha = \sqrt{\frac{1}{k_z} \left(\rho c_p s + q_x^2 k_x + q_y^2 k_y + 2 q_x q_y k_{xy} \right)}, \tag{4}$$

$$\beta = \frac{1}{k_z} \left(q_x k_{xz} + q_y k_{yz} \right). \tag{5}$$

Additionally, we define γ as

$$\gamma = \sqrt{\alpha^2 - \beta^2}. \tag{6}$$

The solution of Eq. (3) can then be written as

$$T^{(n)}(s, q_x, q_y, z) = T_h^{(n)}(s, q_x, q_y, z) + \delta_{nm} T_p^{(n)}(s, q_x, q_y, z), \tag{7}$$

where the homogeneous solution T_h and the particular solution T_p are given by

$$\begin{aligned} T_h^{(n)}(s, q_x, q_y, z) = e^{-i\beta^{(n)}(z-\lambda^{(n)})} e^{-i\lambda_\beta{}^{(n)}} \\ \left(A^{(n)} e^{\gamma^{(n)}(z-\lambda^{(n)}-L^{(n)})} + B^{(n)} e^{-\gamma^{(n)}(z-\lambda^{(n)})} \right), \end{aligned} \tag{8}$$

$$T_p^{(n)}(s, q_x, q_y, z) = \frac{\tilde{Q}_s(q_x, q_y)\tilde{Q}_t(s)}{2k_z^{(n)}\gamma^{(n)}} e^{-i\beta^{(n)}(z-z_0)} e^{-\gamma^{(n)}|z-z_0|} \tag{9}$$

with the abbreviations

$$\lambda^{(n)} = \sum_{i=1}^{n-1} L^{(i)}, \tag{10}$$

$$\lambda_\beta^{(n)} = \sum_{i=1}^{n-1} \beta^{(i)} L^{(i)}. \tag{11}$$

The unknown coefficients $A^{(n)}$ and $B^{(n)}$ for each layer n are then determined by the boundary conditions. Note that we already applied some scaling to those coefficients in Eq. (8) [12]. The main purpose of this scaling is to guarantee that in the end we only have to evaluate exponentials with a negative exponent. Since we expect values of γ with a very large positive real part during the inverse transforms, this avoids problems with numerical overflows.

2.2. Boundary conditions

The heat flux in z-direction is given by

$$\Phi_z = (-\mathbf{K}\nabla T)\,\vec{n}_z = -k_z \left(i\beta + \frac{\partial}{\partial z} \right) T. \tag{12}$$

We begin with the upper and lower boundaries. Here we use Robin-type convective boundary conditions with the heat transfer coefficients h_1 and h_2

for the upper and lower boundaries, respectively. For the upper boundary, we also include a temporally and spatially varying outer fluid temperature T_a, while the outer fluid temperature at the lower boundary is fixed at zero. This results in the following boundary conditions:

$$\left[k_z^{(1)}\left(i\beta^{(1)}+\frac{\partial}{\partial z}\right)T^{(1)}\right]_{z=0}=h_1\left[T^{(1)}-T_a(s,q_x,q_y)\right]_{z=0}, \tag{13}$$

$$\left[k_z^{(N)}\left(i\beta^{(N)}+\frac{\partial}{\partial z}\right)T^{(N)}\right]_{z=\lambda^{(N+1)}}=-h_2T^{(N)}|_{z=\lambda^{(N+1)}}. \tag{14}$$

Note that we have to assume here that the heat transfer coefficients do not depend on time and space. For the interfaces between the layers, we assume a perfect thermal contact. Thus, the boundary conditions for the interface between layer (n) and $(n+1)$ with $n=1,...,(N-1)$ read

$$T^{(n)}|_{z=\lambda^{(n+1)}}=T^{(n+1)}|_{z=\lambda^{(n+1)}}, \tag{15}$$

$$\left[k_z^{(n)}\left(i\beta^{(n)}+\frac{\partial}{\partial z}\right)T^{(n)}\right]_{z=\lambda^{(n+1)}}=\left[k_z^{(n+1)}\left(i\beta^{(n+1)}+\frac{\partial}{\partial z}\right)T^{(n+1)}\right]_{z=\lambda^{(n+1)}}. \tag{16}$$

Inserting the solution (7)-(9) into the boundary conditions (13)-(16) yields after some algebraic manipulation

$$\begin{aligned}&A^{(1)}(\gamma^{(1)}-\frac{h_1}{k_z^{(1)}})e^{(1)}-B^{(1)}(\gamma^{(1)}+\frac{h_1}{k_z^{(1)}})\\&\quad=-\frac{1}{k_z^{(1)}}\left[\delta_{1m}f_2^{(0)}(1-\frac{h_1}{k_z^{(1)}\gamma^{(1)}})+h_1T_0(s,q_x,q_y)\right],\end{aligned} \tag{17}$$

$$\begin{aligned}&A^{(N)}(\gamma^{(N)}+\frac{h_2}{k_z^{(N)}})-B^{(N)}(\gamma^{(N)}-\frac{h_2}{k_z^{(N)}})e^{(N)}\\&\quad=\frac{1}{k_z^{(N)}}\left[\delta_{Nm}f_1^{(N)}(1-\frac{h_2}{k_z^{(N)}\gamma^{(N)}})\right],\end{aligned} \tag{18}$$

$$\begin{aligned}&A^{(n)}+B^{(n)}e^{(n)}-A^{(n+1)}e^{(n+1)}-B^{(n+1)}\\&\quad=-\frac{\delta_{nm}}{k_z^{(n)}\gamma^{(n)}}f_1^{(n)}+\frac{\delta_{(n+1)m}}{k_z^{(n+1)}\gamma^{(n+1)}}f_2^{(n)},\end{aligned} \tag{19}$$

$$\begin{aligned}&A^{(n)}k_z^{(n)}\gamma^{(n)}-B^{(n)}k_z^{(n)}\gamma^{(n)}e^{(n)}\\&\quad-A^{(n+1)}k_z^{(n+1)}\gamma^{(n+1)}e^{(n+1)}+B^{(n+1)}k_z^{(n+1)}\gamma^{(n+1)}\\&\quad=\delta_{nm}f_1^{(n)}+\delta_{(n+1)m}f_2^{(n)},\end{aligned} \tag{20}$$

using the abbreviations

$$e^{(n)} = e^{-\gamma^{(n)} L^{(n)}}, \tag{21}$$

$$f_1^{(n)} = \frac{\tilde{Q}_s(q_x, q_y)\tilde{Q}_t(s)}{2} e^{-(\gamma^{(n)} + i\beta^{(n)})(\lambda^{(n+1)} - z_0)} e^{i\lambda_\beta^{(n+1)}}, \tag{22}$$

$$f_2^{(n)} = \frac{\tilde{Q}_s(q_x, q_y)\tilde{Q}_t(s)}{2} e^{-(\gamma^{(n+1)} - i\beta^{(n+1)})(z_0 - \lambda^{(n+1)})} e^{i\lambda_\beta^{(n+1)}}. \tag{23}$$

Equations (17)-(20) form a pentadiagonal system of linear equations that determines the unknown coefficients, completing the solution in Fourier-Laplace space. We note that the left hand side is similar but not identical to the system found by Zhang *et al.* [11] for the steady-state, isotropic and semi-infinite case.

The pentadiagonal system can also be written in tridiagonal form by replacing equations (19) and (20) by the two equivalent equations

$$\begin{aligned} &A^{(n)}(k_z^{(n+1)}\gamma^{(n+1)} + k_z^{(n)}\gamma^{(n)}) + B^{(n)}(k_z^{(n+1)}\gamma^{(n+1)} - k_z^{(n)}\gamma^{(n)})e^{(n)} \\ &\quad - 2A^{(n+1)}k_z^{(n+1)}\gamma^{(n+1)}e^{(n+1)} \\ &\quad = \delta_{nm} f_1^{(n)}\left(1 - \frac{k_z^{(n+1)}\gamma^{(n+1)}}{k_z^{(n)}\gamma^{(n)}}\right) + 2\delta_{(n+1)m} f_2^{(n)}, \end{aligned} \tag{24}$$

$$\begin{aligned} &-2B^{(n)}k_z^{(n)}\gamma^{(n)}e^{(n)} + A^{(n+1)}(k_z^{(n)}\gamma^{(n)} - k_z^{(n+1)}\gamma^{(n+1)})e^{(n+1)} \\ &\quad + B^{(n+1)}(k_z^{(n)}\gamma^{(n)} + k_z^{(n+1)}\gamma^{(n+1)}) \\ &\quad = 2\delta_{nm} f_1^{(n)} + \delta_{(n+1)m} f_2^{(n)}\left(1 - \frac{k_z^{(n)}\gamma^{(n)}}{k_z^{(n+1)}\gamma^{(n+1)}}\right). \end{aligned} \tag{25}$$

For a fixed number of layers and a specific source layer, this system can be solved analytically. In Appendix A we provide a closed form solution for the important special case of 3 layers with a source placed in the top layer. Otherwise, the system can be solved numerically with $O(N)$ flops.

We can also consider layers moving with a constant velocity in the x-y plane $\vec{u}^{(n)} = (u_x^{(n)}, u_y^{(n)}, 0)^T$. Such a velocity generates an additional heat flux term $\rho c_p \vec{u} T$ [13] and is therefore also handled by the Fourier transform, changing α from (4) to

$$\alpha_u = \sqrt{\frac{1}{k_z}\left(\rho c_p(s + i(q_x u_x + q_y u_y)) + q_x^2 k_x + q_y^2 k_y + 2q_x q_y k_{xy}\right)}. \tag{26}$$

If the same velocity is assigned to all layers, a moving source can be calculated.

3. Transformation to real space

Since the solution presented here is based on integral transforms that are hard to invert analytically given the resulting equations, its usefulness depends on the ability to invert those transforms efficiently using numerical methods. For the inverse Fourier transform and the inverse Laplace transform, we chose two different methods for each transform, where one method is preferable for a low number of evaluation points while the other performs better for a large number of points.

3.1. Inverse Fourier Transform (IFT)

The 2D inverse Fourier transform is given by

$$T(x,y) = \frac{1}{4\pi^2}\int_{-\infty}^{\infty}\int_{-\infty}^{\infty} T(q_x,q_y)e^{i(q_x x+q_y y)}\mathrm{d}q_x\mathrm{d}q_y. \tag{27}$$

If the solution is required for a large number of points in the (x,y)-plane, it is best to distribute points on a sufficiently large regular grid and approximate the inverse transform using FFT-methods [11]. Arbitrary points can then be interpolated between the grid points. If, instead, the solution is needed only for a few spatial points, this is clearly not optimal. Directly discretizing equation (27) using the trapezoidal rule for an arbitrary point however leads to a very slowly convergent sequence, requiring thousands of points per integral to obtain accurate results. Luckily, applying suitable coordinate transformations can tremendously improve the convergence [14]. To make use of this, we first transform equation (27) to polar coordinates (q,Φ_q):

$$T(x,y) = \frac{1}{4\pi^2}\int_{0}^{\infty}\int_{0}^{2\pi} T(q,\Phi_q)e^{iq(x\sin\Phi_q+y\cos\Phi_q)}q\mathrm{d}q\mathrm{d}\Phi_q. \tag{28}$$

Here, the Φ_q-integration already converges quickly using the trapezoidal rule. In order to obtain the same property for the q-integration, we apply the double exponential substitution [15, 16]

$$q = e^{2\sinh\rho}, \tag{29}$$

$$q\mathrm{d}q = 2e^{4\sinh\rho}\cosh\rho\,\mathrm{d}\rho \tag{30}$$

changing the integration limits back to $(-\infty,\infty)$. Due to the sharp drop on both sides, the limits can then be cut to *e.g.* $(-3,3)$.

3.2. Inverse Laplace Transform (ILT)

To invert the Laplace transform, we have to solve the Bromwich integral

$$T(t) = \frac{1}{2\pi i} \int_{\sigma-i\infty}^{\sigma+i\infty} T(s) e^{st} \mathrm{d}s. \tag{31}$$

For single point evaluations, contour deformation methods turned out to be extremely efficient when applicable [17]. Especially the hyperbolic contour method was successfully applied to the optical diffusion equation [18], giving accurate results with merely 15 evaluations of the integrand. Since the optical diffusion equation is very similar to the heat conduction equation, we can expect this method to yield good results here as well. In general however, the optimal parameters for the integration contour depend on the time t. Thus, if the transform is to be evaluated for many values of t, a different method is required that permits calculating the transform for different values of t from the same set of sample points in Laplace space. A powerful method with this property is based on a complex Fourier series for a suitable choice of σ in equation (31), using the quotient-difference algorithm to accelerate the resulting series [19]. This method usually requires more sample points than the hyperbolic contour method ($\sim 30 - 40$), but can quickly generate results for many values of t.

4. Results and discussion

In this section, we compare the solution derived above to numerical solutions of equation (2). We use the COMSOL Multiphysics® software to obtain a numerical solution of the heat transfer equation [20]. The geometry is modeled as stacked cylinders with a radius of 1 m. This radius is large enough to approximate the laterally infinite model used in the semi-analytical solution. The material parameters and boundary conditions are otherwise chosen identical to those in the semi-analytical solution. The semi-analytical solution is implemented in Python and freely available [21] along with the numerical reference solution data. In all these comparisons, the medium and the outer fluid have an initial temperature of $T_0 = 293.15\,\mathrm{K}$. We shift this initial temperature to zero and add T_0 afterwards. This shift is possible, because the heat equation (2) is linear and $T = \mathrm{const}$ solves the corresponding homogeneous equation while being compatible with all imposed boundary conditions, if the shift is applied to the outer fluid temperatures

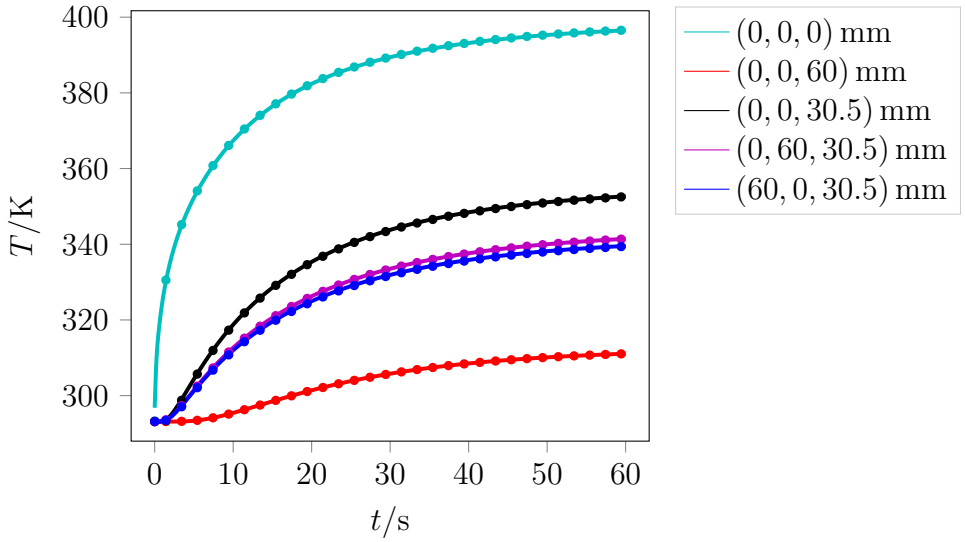

Figure 2: Time dependent temperature at certain points inside a three-layered medium. The solid lines are the results of the semi-analytical solution, the markers represent the numeric reference.

as well. The medium is heated by a source located at the top surface possessing a Gaussian profile with a radius of $r_w = 10\,\mathrm{cm}$ and a total power of $P = 20\,\mathrm{kW}$. Therefore, we have the following source term in Fourier space:

$$\tilde{Q}_s(q_x, q_y) = Pe^{-\frac{1}{4}(q_x^2+q_y^2)r_w^2} = Pe^{-\frac{1}{4}q^2 r_w^2}. \tag{32}$$

This source is switched on at time $t = 0$, which leads to a Laplace domain source term:

$$\tilde{Q}_t(s) = \frac{1}{s}. \tag{33}$$

The heat transfer coefficients are assumed to be $h_1 = 3\,\mathrm{kW\,m^{-2}\,K^{-1}}$ for the top surface and $h_2 = 4\,\mathrm{kW\,m^{-2}\,K^{-1}}$ for the bottom surface. The medium parameters are listed in Appendix B.

As a first example, we use a three-layered medium where the principal axes of all thermal conductivity tensors are oriented along the coordinate axes. The parameters are listed in table B.1. The outer fluid temperature is kept constant at T_0. We calculate the time dependent temperature at specific spatial points inside the medium using the complex Fourier series ILT and the direct integration IFT. The results are given in Figure 2 showing a good agreement of the two solutions. The median values of the relative error

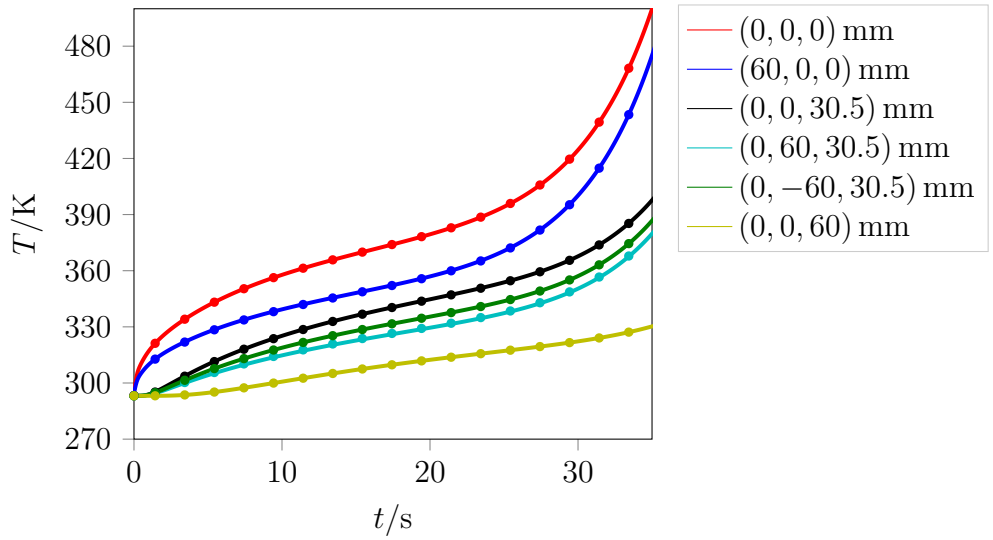

Figure 3: Time dependent temperature at certain points inside a three-layered medium with an exponentially rising outer fluid temperature above the medium. The solid lines are the results of the semi-analytical solution, the markers represent the numeric reference.

magnitudes are between 0.03% and 0.3%. These errors are mainly due to the spatial discretization in the numerical reference solution. Using a finer spatial grid lowers the errors to 0.002% to 0.019%, but greatly increases the calculation time and memory consumption. Larger relative errors can only be observed for very small values of t. This is caused by the numerical inverse Laplace transforms, since both algorithms exploit the s-dependence of the Laplace kernel, which turns to unity for $t = 0$.
Next, we use a three-layered medium with arbitrarily oriented principal axes of the thermal conductivity tensor. The parameters of this medium are listed in table B.2. Here, the outer fluid temperature below the medium is fixed at T_0, while the temperature of the fluid above the medium T_a rises with time t according to

$$T_a(t) = T_0 + (\cosh(at) - 1)\mathrm{K}, \tag{34}$$

with $a = 0.2\,\mathrm{s}^{-1}$. Since we shift the initial medium temperature to 0 and add T_0 afterwards, we get

$$T_a(s) = \frac{s}{s^2 - a^2} - \frac{1}{s} \tag{35}$$

in Laplace space. Using the same transforms as before, we obtain the results shown in Figure 3. Again, the solution agrees well with the numerical refer-

ence solution.
For the next example, we use the same medium again, but with a constant outer fluid temperature T_0 above and below the medium. We are now interested in the upper surface temperature distribution while the medium is heated by a moving source with a constant velocity of $\vec{u} = (-10, 0, 0)^T \mathrm{mm\,s^{-1}}$. Therefore, we assign the velocity $-\vec{u}$ to all three layers. Since we now have to calculate the temperature for many points in the (x, y)-plane, but only for a few points in time, we use the hyperbolic contour ILT and the 2D FFT. The source is again switched on at $t = 0$. Figure 4 shows the surface temperature distribution 10 s later. The effect of the moving source is clearly visible by a shift and stretch in x-direction while the distribution still looks symmetric to the y-axis. This changes for later times. Figure 5 shows the temperature distribution at $t = 60\,\mathrm{s}$. Here, the symmetry is lost due to the anisotropy of the medium. In all cases, a very good agreement between the semi-analytical and numeric solutions is observed.

For our last example, we use a seven-layered medium, again with a constant outer fluid temperature T_0. The medium parameters are listed in tables B.3 and B.4. Here we are interested in the depth penetration of heat into the medium. Therefore, we calculate temperature profiles in z-direction at $x = y = 0$ for different times t. Since there is no transformation involved in z-direction, we compute these curves point-wise using the hyperbolic contour ILT and the direct integration IFT. The results are shown in figure 6. Again, the two solutions agree very well.

5. Summary and conclusion

In this study, the linear time-dependent heat conduction equation was solved in Fourier-Laplace space for a stack of layers with anisotropic thermal conductivities. The solution includes internal sources, convective outer boundaries with spatially and temporally varying outer fluid temperatures and layers with a uniform lateral velocity. The two transforms were inverted using numerical methods. Depending on the required result, different inverse transform algorithms were chosen. This semi-analytical solution was implemented in Python and all calculations were done using a single thread on a standard desktop PC. While there is still a lot of room for optimization, the calculations are already reasonably quick. For example, the calculations in figures 2 and 3 took about 50 ms per curve with 1000 points, using 35 points for the complex Fourier series ILT and 60×25 points for the IFT. If the

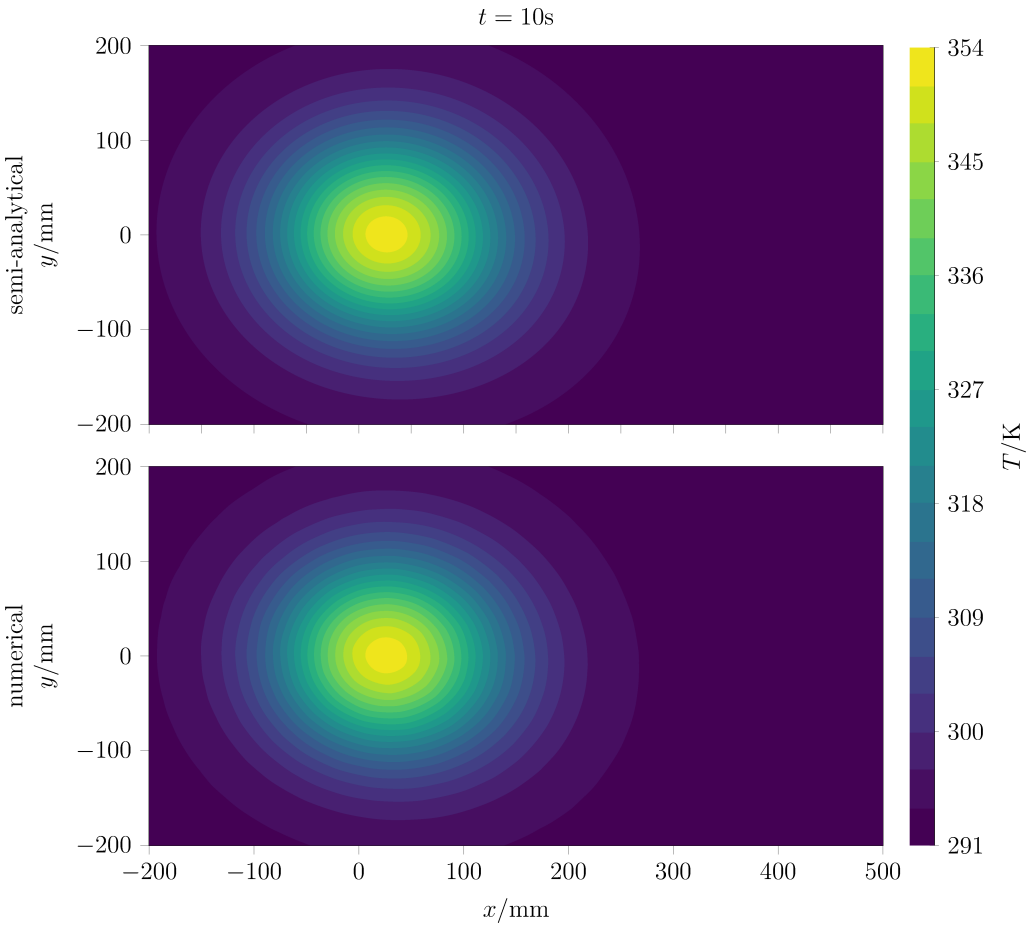

Figure 4: Surface temperature at time $t = 10\,\text{s}$ of a three-layered medium heated by a moving source. The source moves in negative x-direction and was switched on at time $t = 0$.

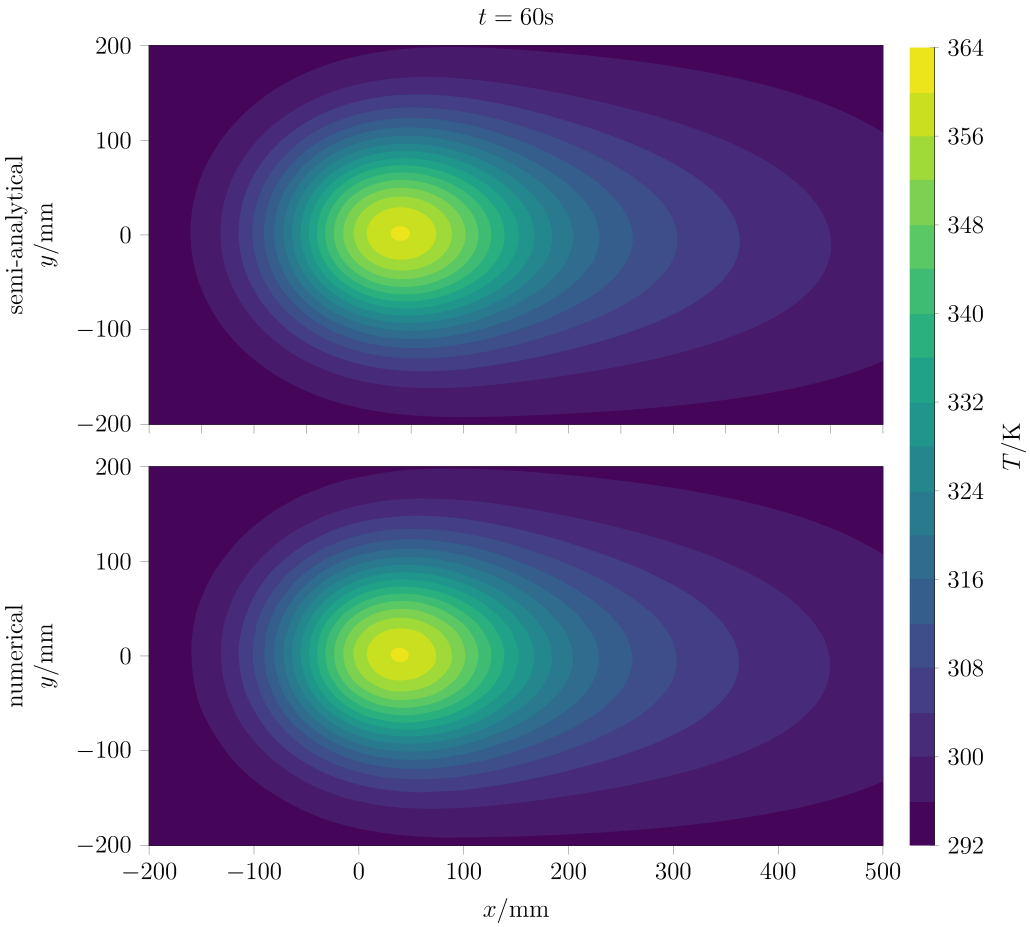

Figure 5: Surface temperature at time $t = 60\,\mathrm{s}$ of a three-layered medium heated by a moving source. The medium anisotropy is clearly visible by the asymmetric temperature distribution.

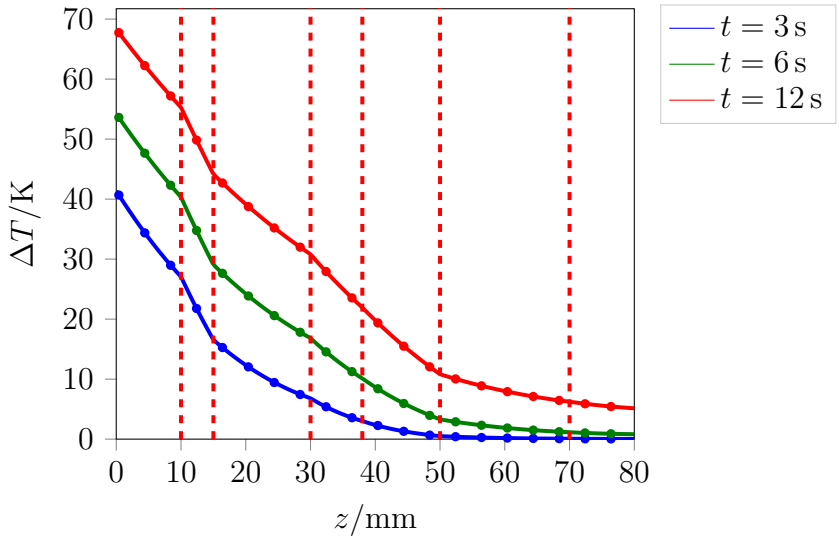

Figure 6: Depth profile of the temperature of a seven-layered medium for different times after the source is switched on. The dashed lines mark the layer boundaries. The solid lines are the results of the semi-analytical solution, the markers represent the numeric reference.

systems of equations are solved numerically instead of using the closed form solution of Appendix A, the time increases to 500 ms. Using seven layers instead of three then results in 600 ms and 28 layers take 1 s per curve. An image in figures 4 and 5 took 4.1 s to compute with the closed form solution, using 15 points for the ILT and a 501×501 points FFT. If the FFT resolution is lowered to 101×101, this time drops to 140 ms. The numerical reference solution took 1.4 h to compute on a similar PC for the 3-layered medium, using 4 cores and 4 GB of RAM. So, while there are powerful numerical solvers available for this kind of problems, the semi-analytical approach explored here can offer a tremendous time saving, especially if the solution is required only for a few points in space or time or if a very high precision is required.

Acknowledgement

This study was supported by Deutsche Forschungsgemeinschaft (grant KI538/17-1).

Appendix A. Explicit 3-layered solution

Here we present a closed form solution of the system of equations (17)-(20) for the special case of $N = 3$ with the source plane inside the first layer. The pentadiagonal system then reads

$$\begin{pmatrix} (\gamma^{(1)}-\frac{h_1}{k_z^{(1)}})e^{(1)} & -(\gamma^{(1)}+\frac{h_1}{k_z^{(1)}}) & 0 & 0 & 0 & 0 \\ 1 & e^{(1)} & -e^{(2)} & -1 & 0 & 0 \\ k_z^{(1)}\gamma^{(1)} & -k_z^{(1)}\gamma^{(1)}e^{(1)} & -k_z^{(2)}\gamma^{(2)}e^{(2)} & k_z^{(2)}\gamma^{(2)} & 0 & 0 \\ 0 & 0 & 1 & e^{(2)} & -e^{(3)} & -1 \\ 0 & 0 & k_z^{(2)}\gamma^{(2)} & -k_z^{(2)}\gamma^{(2)}e^{(2)} & -k_z^{(3)}\gamma^{(3)}e^{(3)} & k_z^{(3)}\gamma^{(3)} \\ 0 & 0 & 0 & 0 & \gamma^{(3)}+\frac{h_2}{k_z^{(3)}} & -(\gamma^{(3)}-\frac{h_2}{k_z^{(3)}})e^{(3)} \end{pmatrix}$$
$$\cdot \begin{pmatrix} A_1 \\ B_1 \\ A_2 \\ B_2 \\ A_3 \\ B_3 \end{pmatrix} = \begin{pmatrix} -\frac{1}{k_z^{(1)}}g_1 \\ -\frac{1}{k_z^{(1)}\gamma^{(1)}}g_2 \\ g_2 \\ 0 \\ 0 \\ 0 \end{pmatrix}, \tag{A.1}$$

with

$$g_1 = (1 - \frac{h_1}{k_z^{(1)}\gamma^{(1)}})f_2^{(0)} + h_1\tilde{T}_a(s, q_x, q_y), \tag{A.2}$$

$$g_2 = f_1^{(1)}. \tag{A.3}$$

Additionally, we introduce the variables

$$p^{(n)} = 1 + (e^{(n)})^2, \tag{A.4}$$

$$m^{(n)} = 1 - (e^{(n)})^2. \tag{A.5}$$

Then, the desired coefficients can be extracted via Cramer's rule and are given by

$$\begin{aligned} A^{(1)} = {} & \frac{1}{Mk_z^{(1)}}(e^{(1)}g_1 + (1 + \frac{h_1}{k_z^{(1)}\gamma^{(1)}})g_2) \\ & \cdot \Big[\gamma^{(2)}k_z^{(2)}(\gamma^{(3)}p^{(3)} + \frac{h_2}{k_z^{(3)}}m^{(3)})(\gamma^{(1)}k_z^{(1)}p^{(2)} - \gamma^{(2)}k_z^{(2)}m^{(3)}) \\ & +\gamma^{(3)}k_z^{(3)}(\gamma^{(3)}m^{(3)} + \frac{h_2}{k_z^{(3)}}p^{(3)})(\gamma^{(1)}k_z^{(1)}m^{(2)} - \gamma^{(2)}k_z^{(2)}p^{(2)})\Big], \end{aligned} \tag{A.6}$$

$$
\begin{aligned}
B^{(1)} = & \frac{1}{\gamma^{(1)} k_z^{(1)} M} \Bigg[\gamma^{(2)} k_z^{(2)} (\gamma^{(3)} p^{(3)} + \frac{h_2}{k_z^{(3)}} m^{(3)}) \\
& \Bigg(\gamma^{(1)} k_z^{(1)} p^{(2)} (\gamma^{(1)} (g_1 + e^{(1)} g_2) - \frac{h_1}{k_z^{(1)}} e^{(1)} g_2) \\
& + \gamma^{(2)} k_z^{(2)} m^{(2)} (\gamma^{(1)} (g_1 - e^{(1)} g_2) + \frac{h_1}{k_z^{(1)}} e^{(1)} g_2) \Bigg) \\
& + \gamma^{(3)} k_z^{(3)} (\gamma^{(3)} m^{(3)} + \frac{h_2}{k_z^{(3)}} p^{(3)}) \\
& \Bigg(\gamma^{(1)} k_z^{(1)} m^{(2)} (\gamma^{(1)} (g_1 + e^{(1)} g_2) - \frac{h_1}{k_z^{(1)}} e^{(1)} g_2) \\
& + \gamma^{(2)} k_z^{(2)} p^{(2)} (\gamma^{(1)} (g_1 - e^{(1)} g_2) + \frac{h_1}{k_z^{(1)}} e^{(1)} g_2) \Bigg) \Bigg],
\end{aligned} \tag{A.7}
$$

$$
\begin{aligned}
A^{(2)} = & \frac{2}{M} e^{(2)} (\gamma^{(1)} (e^{(1)} g_1 + g_2) + \frac{h_1}{k_z^{(1)}} g_2) \\
& \left[\gamma^{(2)} k_z^{(2)} (\gamma^{(3)} p^{(3)} + \frac{h_2}{k_z^{(3)}} m^{(3)}) - \gamma^{(3)} k_z^{(3)} (\gamma^{(3)} m^{(3)} + \frac{h_2}{k_z^{(3)}} p^{(3)}) \right],
\end{aligned} \tag{A.8}
$$

$$
\begin{aligned}
B^{(2)} = & \frac{2}{M} (\gamma^{(1)} (e^{(1)} g_1 + g_2) + \frac{h_1}{k_z^{(1)}} g_2) \\
& \left[\gamma^{(2)} k_z^{(2)} (\gamma^{(3)} p^{(3)} + \frac{h_2}{k_z^{(3)}} m^{(3)}) + \gamma^{(3)} k_z^{(3)} (\gamma^{(3)} m^{(3)} + \frac{h_2}{k_z^{(3)}} p^{(3)}) \right],
\end{aligned} \tag{A.9}
$$

$$
A^{(3)} = \frac{4}{M} \gamma^{(2)} k_z^{(2)} e^{(2)} e^{(3)} (\gamma^{(1)} (e^{(1)} g_1 + g_2) + \frac{h_1}{k_z^{(1)}}) (\gamma^{(3)} - \frac{h_2}{k_z^{(3)}}), \tag{A.10}
$$

$$
B^{(3)} = \frac{4}{M} \gamma^{(2)} k_z^{(2)} e^{(2)} (\gamma^{(1)} (e^{(1)} g_1 + g_2) + \frac{h_1}{k_z^{(1)}}) (\gamma^{(3)} + \frac{h_2}{k_z^{(3)}}), \tag{A.11}
$$

where the common denominator M is given by

$$
\begin{aligned}
M = (\gamma^{(1)})^2 k_z^{(1)} m^{(1)} & \left[\gamma^{(2)} k_z^{(2)} p^{(2)} (\gamma^{(3)} p^{(3)} + \frac{h_2}{k_z^{(3)}} m^{(3)}) \right. \\
& \left. + \gamma^{(3)} k_z^{(3)} m^{(2)} (\gamma^{(3)} m^{(3)} + \frac{h_2}{k_z^{(3)}} p^{(3)} \right] \\
& + \gamma^{(2)} k_z^{(2)} \frac{h_1}{k_z^{(1)}} m^{(1)} \left[\gamma^{(2)} k_z^{(2)} m^{(2)} (\gamma^{(3)} p^{(3)} + \frac{h_2}{k_z^{(3)}} m^{(3)}) \right. \\
& \left. + \gamma^{(3)} k_z^{(3)} p^{(3)} (\gamma^{(3)} m^{(3)} + \frac{h_2}{k_z^{(3)}} p^{(3)} \right] \\
& + \gamma^{(1)} p^{(1)} \left[\gamma^{(2)} k_z^{(2)} (\gamma^{(3)} p^{(3)} + \frac{h_2}{k_z^{(3)}} m^{(3)}) (h_1 p^{(2)} + \gamma^{(2)} k_z^{(2)} m^{(2)}) \right. \\
& \left. + \gamma^{(3)} k_z^{(3)} (\gamma^{(3)} m^{(3)} + \frac{h_2}{k_z^{(3)}} p^{(3)}) (h_1 m^{(2)} + \gamma^{(2)} k_z^{(2)} p^{(2)}) \right] .
\end{aligned}
\tag{A.12}
$$

Appendix B. Medium parameters

Table B.1: Three-layered medium with all principal axes oriented along the coordinate axes.

Layer	$\rho(\mathrm{kg\,m^{-3}})$	$c_p(\mathrm{J\,kg^{-1}\,K^{-1}})$	$k(\mathrm{W\,m^{-1}\,K^{-1}})$			$l(\mathrm{mm})$
			k_{xx}	k_{yy}	k_{zz}	
1	2730	893	200	400	155	30
2	1150	1700	20	20	20	5
3	2730	893	400	200	155	25

Table B.2: Thermal conductivities of a modified three-layered medium with arbitrarily oriented principal axes.

Layer	$k(\mathrm{W\,m^{-1}\,K^{-1}})$					
	k_{xx}	k_{xy}	k_{xz}	k_{yy}	k_{yz}	k_{zz}
1	150	$-50\sqrt{3}$	50	250	$-50\sqrt{3}$	300
2	$\frac{235}{8}$	$-\frac{25}{8}\sqrt{3}$	$\frac{15}{4}$	$\frac{185}{8}$	$-\frac{5}{4}\sqrt{3}$	$\frac{75}{2}$
3	150	$-50\sqrt{3}$	-50	250	$50\sqrt{3}$	300

Table B.3: Seven-layered medium parameters. The thermal conductivities are listed in table B.4

Layer	$\rho(\mathrm{kg\,m^{-3}})$	$c_p(\mathrm{J\,kg^{-1}\,K^{-1}})$	$l(\mathrm{mm})$
1	2730	893	10
2	1150	1700	5
3	2730	893	15
4	2730	893	8
5	2730	893	12
6	2730	893	20
7	2730	893	10

Table B.4: Thermal conductivities of the seven-layered medium.

Layer	$k(\mathrm{W\,m^{-1}\,K^{-1}})$					
	k_{xx}	k_{xy}	k_{xz}	k_{yy}	k_{yz}	k_{zz}
1	150	$-50\sqrt{3}$	50	250	$-50\sqrt{3}$	300
2	$\frac{235}{2}$	$-\frac{25}{2}\sqrt{3}$	15	$\frac{185}{2}$	$-5\sqrt{3}$	150
3	150	$-50\sqrt{3}$	-50	250	$50\sqrt{3}$	300
4	$\frac{675}{4}$	$-\frac{75}{4}\sqrt{3}$	$-\frac{25}{2}\sqrt{3}$	$\frac{825}{4}$	$\frac{75}{2}$	175
5	155	0	0	155	0	155
6	425	-25	$25\sqrt{6}$	425	$-25\sqrt{6}$	350
7	250	0	0	150	0	300

References

[1] S. Suresh, A. Mortensen, Fundamentals of Functionally Graded Materials: Processing and Thermomechanical Behaviour of Graded Metals and Metal-ceramic Composites, IOM Communications Limited, 1998.

[2] Y. Miyamoto, W. Kaysser, B. Rabin, A. Kawasaki, R. Ford, Functionally Graded Materials: Design, Processing and Applications, Springer US, 1999.

[3] M. Naebe, K. Shirvanimoghaddam, Functionally graded materials: A review of fabrication and properties, Applied Materials Today 5 (2016) 223 – 245.
URL http://doi.org/10.1016/j.apmt.2016.10.001

[4] M. Tkadletz, N. Schalk, R. Daniel, J. Keckes, C. Czettl, C. Mitterer, Advanced characterization methods for wear resistant hard coatings: A review on recent progress, Surface and Coatings Technology 285 (2016) 31 – 46.
URL http://doi.org/10.1016/j.surfcoat.2015.11.016

[5] L. Qiu, et al., Remarkably enhanced thermal transport based on a flexible horizontally-aligned carbon nanotube array film, Scientific Reports 6 (2016) 21014.
URL http://doi.org/10.1038/srep21014

[6] P. H. M. Böttger, L. Braginsky, V. Shklover, E. Lewin, J. Patscheider, D. G. Cahill, M. Sobiech, Hard wear-resistant coatings with anisotropic thermal conductivity for high thermal load applications, Journal of Applied Physics 116 (1) (2014) 013507.
URL http://doi.org/10.1063/1.4886182

[7] M. V. Griffith, G. K. Horton, The transient flow of heat through a two-layer wall, Proceedings of the Physical Society 58 (4) (1946) 481.
URL http://doi.org/10.1088/0959-5309/58/4/318

[8] W. Chester, R. Bobone, E. Brocher, Transient conduction through a two-layer medium, International Journal of Heat and Mass Transfer 27 (11) (1984) 2167 – 2170.
URL http://doi.org/10.1016/0017-9310(84)90205-9

[9] N. Simões, A. Tadeu, Fundamental solutions for transient heat transfer by conduction and convection in an unbounded, half-space, slab and layered media in the frequency domain, Engineering Analysis with Boundary Elements 29 (12) (2005) 1130 – 1142.
URL http://doi.org/10.1016/j.enganabound.2005.06.002

[10] J. von Wolfersdorf, Influence of lateral conduction due to flow temperature variations in transient heat transfer measurements, International Journal of Heat and Mass Transfer 50 (5) (2007) 1122 – 1127.
URL http://doi.org/10.1016/j.ijheatmasstransfer.2006.06.049

[11] H. Zhang, W. Wang, S. Zhang, Z. Zhao, Semi-analytic solution of three-dimensional temperature distribution in multilayered materials based on explicit frequency response functions, International Journal of

Heat and Mass Transfer 118 (2018) 208 – 222.
URL http://doi.org/10.1016/j.ijheatmasstransfer.2017.10.118

[12] A. Liemert, Analytische Lösungen der Strahlungstransfergleichung und ihrer Approximationen, Ph.D. thesis, Universität Ulm (2011).

[13] H. Carslaw, J. Jaeger, Conduction of heat in solids, Oxford science publications, Clarendon Press, 1959.

[14] L. N. Trefethen, J. A. C. Weideman, The exponentially convergent trapezoidal rule, SIAM Review 56 (2014) 385 – 458.
URL http://doi.org/10.1137/130932132

[15] H. Takahasi, M. Mori, Double exponential formulas for numerical integration, Publications of the Research Institute for Mathematical Sciences 9 (1974) 721 – 741.

[16] W. H. Press, S. A. Teukolsky, W. T. Vetterling, B. P. Flannery, Numerical Recipes 3rd Edition: The Art of Scientific Computing, 3rd Edition, Cambridge University Press, New York, 2007.

[17] J. A. C. Weideman, L. Trefethen, Parabolic and hyperbolic contours for computing the bromwich integral, Mathematics of Computation 76 (2007) 1341–1356.
URL http://doi.org/10.1090/S0025-5718-07-01945-X

[18] A. Liemert, A. Kienle, Application of the laplace transform in time-domain optical spectroscopy and imaging, Journal of Biomedical Optics 20 (2015) 110502.
URL http://doi.org/10.1117/1.JBO.20.11.110502

[19] L. Brancik, Numerical inverse laplace transforms for electrical engineering simulation, in: K. Perutka (Ed.), MATLAB for Engineers, InTech, London, 2011, Ch. 3, pp. 51 – 74.

[20] COMSOL AB, Comsol multiphysics® v5.2a, www.comsol.com.

[21] D. Reitzle, aniso_heat v1.0 (2019). doi:10.5281/zenodo.2536140.